JOURNAL OF CATALYSIS **158,** 236–250 (1996)
ARTICLE NO. 0023

Chemical and Physical Characterization of Alumina-Supported Chromia-Based Catalysts and Their Activity in Dehydrogenation of Isobutane

F. Cavani,* M. Koutyrev,*,[1] F. Trifirò,*,[2] A. Bartolini,† D. Ghisletti,† R. Iezzi,† A. Santucci,† and G. Del Piero‡

*Dipartimento di Chimica Industriale e dei Materiali, Università di Bologna, Viale Risorgimento 4, 40136 Bologna, Italy; †Snamprogetti SpA, Research Laboratories, Via Maritano 26, 20097 San Donato Milan, Italy; and ‡Eniricerche SpA, Via Maritano 26, 20097 San Donato Milan, Italy

Received April 5, 1995; revised June 26, 1995; accepted August 24, 1995

Dehydrogenation catalysts based on chromium oxide supported on commercial alumina which contained increasing amounts of chromium oxide were prepared and characterized with different techniques: XPS, UV–Vis–NIR diffuse reflectance spectroscopy, XRD, and chemical analysis. Potassium-doped catalysts containing increasing amounts of alkali metal also were prepared and characterized. The reactivity of the samples in isobutane dehydrogenation was tested, and the effect of chromium and potassium loading was examined. The results were analyzed and compared with data from the scientific literature in order to draw up a model of this catalytic system. It is proposed that in samples calcined at 600°C an initial coverage of the alumina support occurs, constituted of Cr^{6+} species anchored to the support, and of dispersed Cr^{6+} and Cr^{3+} oxide species. This latter Cr^{6+} species could be removed by a treatment with water, and thus was not grafted to the support. Crystalline α-Cr_2O_3 was found only for the higher chomium oxide loading. In spent catalysts all the chromium was present in the Cr^{3+} form; the Cr^{3+} species formed by reduction in the reaction environment of the Cr^{6+} species were less active than the Cr^{3+} species in dispersed Cr^{3+} oxide. The activity was found to be proportional to the overall amount of chromium, except for the highest CrO_3 loading (15.3 wt% CrO_3) which showed a lower activity. The addition of potassium led to the formation of a potassium chromate phase, the formation of which occurred at the expense of the dispersed Cr^{3+} oxide and of α-Cr_2O_3. The catalytic activity was generally inhibited by the addition of potassium, except for the catalyst containing 15.3 wt% CrO_3. In this case an increase in activity was achieved by addition of amounts of potassium lower than 1 wt% K_2O.

INTRODUCTION

Supported chromium oxide-based catalysts find industrial application for different reactions, such as polymerization of ethylene (1, 2) and dehydrogenation of paraffins (3). In addition, they are known to be active in the selective oxidation of alcohols (4).

Wide interest was given some decades ago to this catalytic system when dehydrogenation of *n*-butane was the main source for the synthesis of butenes and butadiene (5). Renewed interest has developed in recent years due to the increased need for isobutene for MTBE synthesis, but also because of the possibility to compete with high-capital-investment steam-cracking for the synthesis of pure light olefins for specific applications, such as the synthesis of high-purity propylene and butenes for the polymer industry.

There are several industrial processes available for the dehydrogenation of isobutane to isobutene (3), some of which (the Catofin, the Linde, and the Snamprogetti–Yarsintez processes) employ supported chromium oxide as the catalyst; a dopant, consisting of an alkali metal, is also added to promote activity and/or selectivity to the olefin. Alumina is the preferred support for industrial application, but zirconia also has been studied for this purpose due to its properties of high thermal stability and low surface acidity.

Numerous papers have been published in the literature regarding the characterization of chromium oxide on different supports (6–28). Many works have dealt with the use of a specific technique (e.g., UV–Vis diffuse reflectance spectroscopy (DRS), laser Raman spectroscopy, X-ray photoelectron spectroscopy (XPS)) to characterize supported-chromium oxide catalysts. The effects of the type of support and of some preparation parameters (calcination temperature, chromium oxide loading) on the nature of the chromium species have been the object of most of these investigations. However, complete characterization of these catalysts using a combination of several techniques which could give a better picture of such systems and a thorough examination of the relationships between activity

[1] On leave from the Semenov Institute of Chemical Physics, Russian Academy of Sciences, Moscow, Russia.

[2] To whom correspondence should be addressed.

0021-9517/96 $12.00

in dehydrogenation of paraffins and chromium species in an industrial-like catalyst have not yet been reported. Furthermore, some questions concerning, for example, the role of the alkali metal are still unanswered.

The objective of the research reported here was to study the chemical-physical and catalytic properties in dehydrogenation of isobutane of catalysts prepared by supporting increasing amounts of chromium oxide on a commercial alumina, both in the presence and in the absence of potassium as the dopant. The catalytic tests were carried out at a lower temperature than that used industrially and in the presence of a diluent in order to minimize the influence of coke formation on catalytic performance. The results obtained are compared with data from the scientific literature in an effort to form a better picture of this important catalytic system.

EXPERIMENTAL

Catalysts were prepared by simultaneous impregnation (incipient wetness technique) of a commercial alumina with potassium and chromium, from an aqueous solution containing CrO_3 and K_2CrO_4. The alumina support was characterized by a surface area of 80 m^2/g; particle size ranged from 30 to 150 μm. The samples were then dried overnight at 120°C and calcined at 600°C for 6 h. The amounts of metal oxide with which the alumina samples were impregnated are reported as wt% CrO_3 and of K_2O with respect to the sum of CrO_3, K_2O, and Al_2O_3.

The catalytic tests were carried out in a laboratory, tubular-flow, stainless steel reactor, at atmospheric pressure. Typical test conditions were the following: temperature 470°C, residence time 0.3 or 1.35 s, feed composition: isobutane 5 mol%, remainder helium. The catalyst (0.5 g) used was pelletized in the form of particles ranging from 0.3 to 0.5 mm in size. The reaction products were analyzed online using a Carlo Erba gas chromatograph, equipped with an FID. The only product obtained under the test conditions used (isobutene, with traces of lighter hydrocarbons) was separated from unconverted isobutane by means of a column packed with SP-1700 on Chromosorb PAW; the oven temperature was kept at 40°C.

Several techniques were utilized for the characterization: chemical analysis (titrimetric analysis), UV–Vis–NIR DRS, XPS, XRD, and surface area measurements (BET, single-point method, by adsorption of nitrogen).

Chemical analysis of chromium was done according to the following procedure. First, the calcined sample was treated with water to solubilize chromium species which were not chemically bound to the alumina; in this step Cr^{6+} oxide compounds are dissolved, while Cr_2O_3 is not. The Cr^{6+} species in the two fractions, the dissolved fraction and that bound to the alumina, can be volumetrically titrated with the iodometric method. The amount of Cr^{3+} was determined as the difference between the Cr^{6+} and the total chromium loaded. An approximate estimate of the experimental error of this technique has been evaluated by repeated analysis, and has been found to correspond to approximately 10% of the average value.

The X-ray diffraction (XRD) patterns were collected by means of a computer-controlled Philips goniometer, using Ni-filtered Cu$K\alpha$ radiation (λ = 0.15418 nm). Quantitative evaluation of the amount of crystalline α-Cr_2O_3 was carried out by using the ''matrix flushing method'' developed by Chung (29).

UV–Vis–NIR DR spectra were recorded at room temperature using a Perkin-Elmer Lambda 19 spectrometer, equipped with a 60-mm integrating sphere coated with barium sulphate reflective paint. The Kodak White Reflectance Standard was employed as the reference. Both sample and reference powder were contained in Suprasil quartz cell. The spectra are displayed as apparent absorbance vs wavelength. Due to the absorbance properties of the barium sulphate in the UV and to the fact that the absolute transmittance of the reference material is certified up to 250 nm, the portion of the spectra between 200 and 250 nm is to be considered indicative only.

XPS spectra were recorded with a VG Escalab 200-C spectrometer using Mg$K\alpha$ radiation (1253.6 eV). The base pressure in the analysis chamber was kept in the range 1×10^{-9}–5×10^{-10} mbar. Energy scales were referred to the Al 2*p* peak, which was assumed to have a binding energy of 73.9 eV. The sample treatments were all carried out *in situ* in a high pressure gas cell directly connected to the ultra high vacuum system. The calcined samples were pretreated in synthetic air (1.1 bar, 500°C) in order to obtain comparable and reproducible surface conditions. All reduction treatments were carried out with 20% H_2 in N_2 (1.1 bar, 500°C). The Cr 2*p* region was acquired at the beginning of each experiment and in the shortest time possible in order to avoid the X-ray induced reduction of Cr^{6+}. The surface concentrations of the elements are expressed as intensity peak ratios; therefore, reported trends are only semi-quantitative.

RESULTS

The Nature of Chromium Species in Calcined Catalysts

Characterization by chemical analysis and XRD. Samples were prepared by impregnation of amounts of chromium oxide in the range 1.5–15.3 wt% CrO_3. No change in the value of surface area occurred with respect to the support alone, except for a slight decrease in the surface area of the sample with the highest CrO_3 content (75 vs 80 $m^2\ g^{-1}$). This indicates that deposition of the chromium oxide did not cause any plugging of the alumina pores.

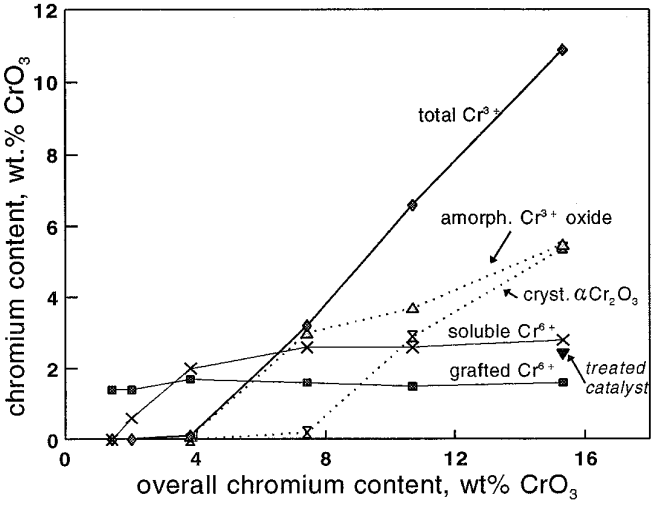

FIG. 1. Amounts of the different chromium species as functions of the overall chromium oxide content in calcined catalysts. "Treated catalyst" refers to the amount of soluble Cr^{6+} in a sample that has been first treated with water to remove soluble Cr^{6+} and then calcined again at 600°C.

Chemical analysis showed the presence of three different chromium species in the catalysts calcined in air at 600°C: (i) a Cr^{3+} species; (ii) a Cr^{6+} species that could be selectively removed by treating the catalyst with cold water, and therefore does not chemically interact with the alumina; (iii) a grafted Cr^{6+} species that is chemically bound to the support. This species was not removed by the treatment with cold water.

The relative amounts of the three species in calcined catalysts are plotted in Fig. 1. At low chromium oxide loading (less than 2 wt% CrO_3) all the oxide was in the form of grafted Cr^{6+}, not dissolved by the preliminary treatment with water. The amount of this species, however, reached a maximum (1.5 wt%) and did not increase further even at the highest loading of chromium oxide. For CrO_3 contents higher than 2 wt%, the amount of soluble Cr^{6+} steadily increased up to a content of 2 wt% (reached for an overall CrO_3 content of 4 wt%). For even higher CrO_3 contents, the increase in this species was much less marked. Finally, for overall CrO_3 loadings higher than 4 wt% Cr^{3+} was also found, and its content increased linearly with increasing chromium oxide loading. This species was not dissolved by the treatment with water.

Also reported in Fig. 1 is the value obtained by first treating the calcined 15.3 wt% CrO_3 catalyst with water, in order to remove the soluble Cr^{6+} selectively, and then calcining the catalyst again at 600°C. The amount of soluble Cr^{6+} was restored at the expense of the Cr^{3+} species, which correspondingly decreased by a similar amount.

Figure 2 shows the X-ray diffraction patterns of calcined samples at increasing CrO_3 contents. Besides the many reflections relative to the alumina (a mixture of three phases), the only reflections attributable to chromium oxide are typical for α-Cr_2O_3. The amount of crystalline α-Cr_2O_3, as detected by XRD, was the following (expressed as wt% CrO_3): 0% at 4.6 wt% total CrO_3, traces at 7.4 wt% total CrO_3, 2.9 ± 0.2 wt% at 10.7 wt% total CrO_3, and 5.4 ± 0.4 wt% at 15.3 wt% total CrO_3. These amounts are lower than the amount of Cr^{3+} determined by chemical analysis (Fig. 1), indicating the presence of undetected Cr^{3+} oxide, present in forms other than crystalline α-Cr_2O_3. The amount of crystalline α-Cr_2O_3 and of undetected Cr^{3+} oxide (determined by difference between the overall amount of Cr^{3+} oxide, determined by titration, and the amount of crystalline α-Cr_2O_3, determined by X-ray diffraction) is also reported in Fig. 1. It is evident that the first-formed Cr^{3+} is spread in an amorphous or microcrystalline (XRD undetectable) phase, and that crystalline α-Cr_2O_3 only forms for CrO_3 contents higher than approximately 7–8 wt%.

Figure 3 reports the amount of grafted Cr^{6+} determined in a series of samples prepared by impregnation of the same amount of chromium oxide (15.3 wt% CrO_3) over aluminas characterized by different crystalline structures and different surface areas. In particular the δ-alumina had a surface area of 150 $m^2\ g^{-1}$, and the γ-alumina of 300 $m^2\ g^{-1}$. It is seen that the amount of Cr^{6+} grafted to the surface was proportional to the surface area, and was in any case lower than the amount that would theoretically be necessary to complete the coverage of the alumina surface. If we refer to the value reported by other authors for the monolayer coverage (9), which corresponds to approximately 0.05 wt% per square meter of support, the fraction of surface coverage occupied by the grafted Cr^{6+} species is approximately 50% in all samples. The discharged catalysts, after reaction, were completely reduced; no amount of Cr^{6+} could be determined by titration.

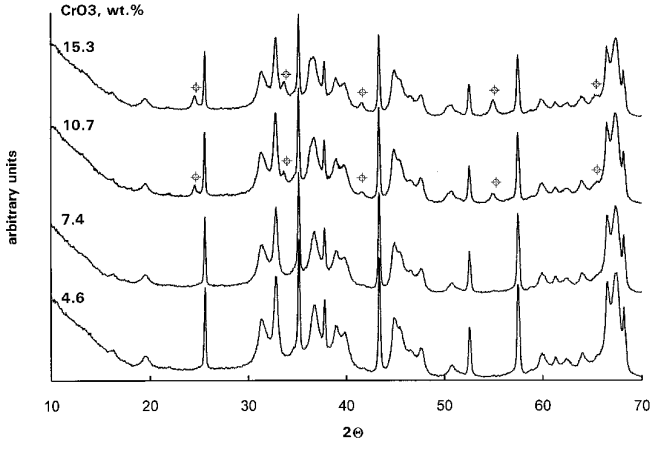

FIG. 2. X-ray diffraction patterns of calcined samples at increasing CrO_3 content (⊕ α-Cr_2O_3).

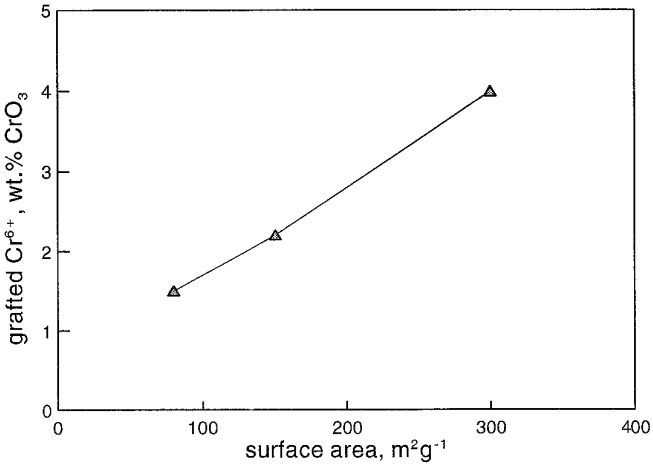

FIG. 3. Amount of grafted Cr^{6+} species as a function of the alumina surface area in different catalysts containing 15.3 wt% CrO_3.

TABLE 1

XPS Binding Energies for Catalysts Calcined at 600°C, with Different CrO_3 Contents

Sample (wt% CrO_3)	Cr^{3+} (eV[a])	Cr^{6+} (eV[a])	total-Cr/Al	Cr^{3+}/Cr^{6+}
4.6	576.6	579.1	1.4	1.4
10.7	576.7	579.2	2.8	1.8
15.3	576.7	579.3	3.9	2.7
15.3 reduced in H_2/N_2	576.4	—	3.6	—
	Reference compounds			
Cr_2O_3	576.6			
CrO_3 (ref. 31)		579.9		
K_2CrO_4		579.1		
$K_2Cr_2O_7$		579.3		

[a] Binding energy of Cr 2*p*3/2 peak.

XPS Characterization. Figure 4a shows the XPS spectra in the Cr 2*p* region for catalysts at increasing CrO_3 loading. The Cr 2*p*3/2 peak was elaborated by introducing constraints providing physical consistency and by taking into account the multiplet splitting due to the unpaired *d* electrons in the valence levels of Cr^{3+} states (29) for the fitting procedure. This procedure made it possible to find only the Cr^{6+} and Cr^{3+} states (Fig. 4b). The oxidation states of chromium were determined by comparing the binding energy of the Cr 2*p*3/2 peak and the value of spin-orbit splitting Cr 2*p*1/2–Cr 2*p*3/2 with reference samples and literature values (18, 30–35). The binding energy and the spin-orbit splitting fall in the range 576.4–576.9 eV and 9.7–9.9 eV, respectively, for Cr^{3+} and in the range 579.1–579.6 eV and 9.0–9.2 eV, respectively, for Cr^{6+}, in agreement with values reported in the literature. It is very difficult to ascertain the contribution of intermediate chromium states in the Cr 2*p*3/2 region due to both the high chromia loadings and the intrinsic complexity of the Cr^{3+} component (18, 33, 34).

Table 1 summarizes chromium data measured for calcined catalysts with increasing amounts of CrO_3. The overall amount of chromium detected at the catalyst surface increased almost linearly as the loading increased, as shown by the intensity ratio between the Cr 2*p*3/2 peak and the Al 2*p* peak. This suggests that the chromium is well dispersed over the entire range of CrO_3 content. Moreover, as the overall chromia loading increased, different distributions between surface Cr^{3+} and Cr^{6+} states occurred leading to higher Cr^{3+}/Cr^{6+} intensity ratios. Similar results have been obtained by other authors (32, 34) for supported chromium oxide.

Assuming the same relative sensitivity factor for Cr^{3+} and Cr^{6+} (36), the Cr^{3+}/Cr^{6+} intensity ratios reported in Table 1 represent quantitative values of the surface concentrations. If we compare the surface Cr^{3+}/Cr^{6+} concentration ratios with the results of the bulk analysis, we find that the values (1.8, 2.7) obtained for the samples with high CrO_3

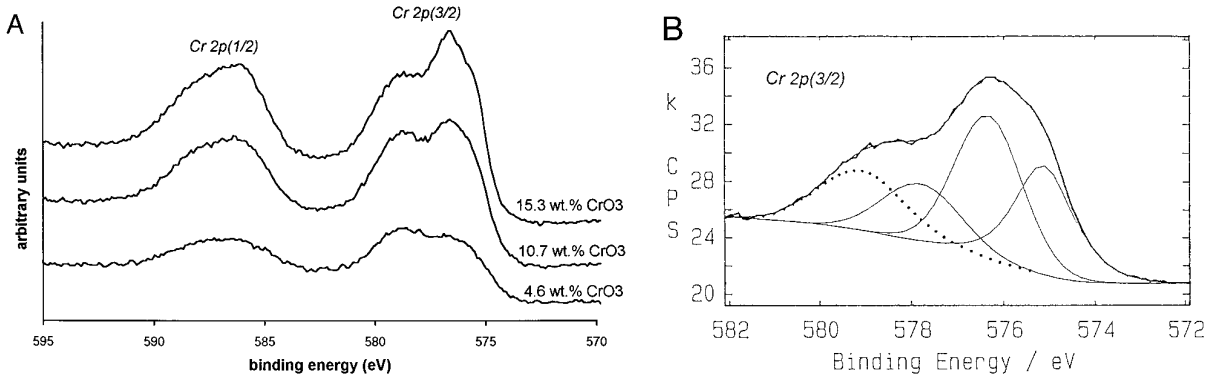

FIG. 4. (a) XPS spectra of Cr 2*p* level for calcined catalysts at increasing CrO_3 loading. (b) Cr 2*p*3/2 region peak fitting for 15.3 wt% CrO_3 catalyst showing the multiplet structure of Cr^{3+} (solid lines) and the Cr^{6+} component (dot line).

TABLE 2

XPS Binding Energies for the 15.3 wt% CrO_3 Catalyst after Different Treatments

Treatment	Cr^{3+} (eV[a])	Cr^{6+} (eV[a])	total-Cr/Al	Cr^{3+}/Cr^{6+}
Calcined	576.7	579.3	3.9	2.7
Washed	576.9	579.3	3.0	16.7
Washed and reduced, 500°C	576.4	—	3.1	—
Washed and oxidized, 500°C	576.8	579.6	3.5	3.4

[a] Binding energy of Cr 2*p*3/2 peak.

content are very close to those determined by chemical analysis (1.60 and 2.50, respectively), while for the sample with the lower CrO_3 content the Cr^{3+}/Cr^{6+} intensity ratio (1.4) is much higher than the bulk value (0.20). The relatively high amounts of surface Cr^{3+} at low chromium oxide loadings, in contrast with that determined by chemical analysis, might be explained by hypothesizing that the Cr^{3+} oxide formed first is highly dispersed in an almost amorphous, microcrystalline surface environment, which leads to the detection of a high fraction of it by means of XPS.

Treatment with water of the sample containing 15.3 wt% CrO_3 led to a decrease in the overall intensity of the Cr 2*p*3/2 signal relative to that of the Al 2*p* peak due to the removal of surface Cr^{6+} species (Table 2). The signal of Cr^{6+} in the Cr 2*p*3/2 peak is depressed considerably in the washed sample compared with the untreated one (Fig. 5) even though a weak component remains. The presence of a residual Cr^{6+} component in the washed sample is revealed by the further signal depression in the high binding energy side of the spectrum occurring after H_2 reduction. If the washed catalyst is then oxidized in air, the amount of Cr^{6+} is in great part restored. The oxidation treatment also leads to a surface redistribution of chromium, as evidenced by the modification of the total-Cr/Al 2*p* ratio (Table 2).

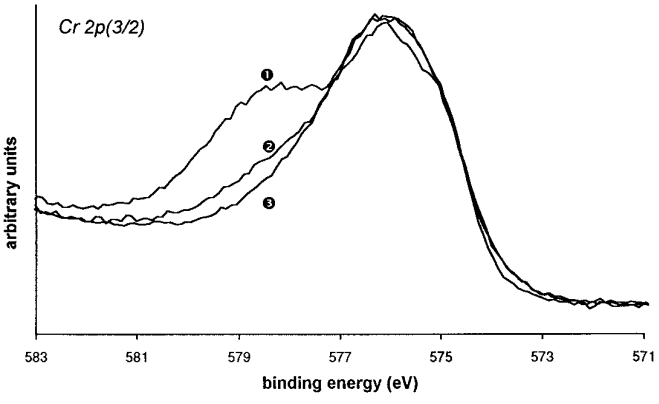

FIG. 5. Cr 2*p*3/2 signal in the 15.3 wt% CrO_3 calcined catalyst (1), after treatment with water (2), and after treatment and subsequent reduction in H_2 (3).

All the samples subjected to the H_2 reduction treatment gave spectra in which the signal relative to Cr^{6+} is absent and only the Cr^{3+} signal is seen.

Similar results in alumina-supported chromium oxide-based catalysts calcined at 550°C have been reported by Grünert *et al.* (18). When the catalysts were reduced for a long time, however, the Cr^{3+} signal and the signal attributed to highly dispersed zerovalent chromium (571.7–572.0 eV) were detected, while Cr^{2+} and Cr^{5+} were not found. The authors also reported that the reduction of surface Cr^{6+} led to a chromium redispersion. Jagannathan *et al.* (34) reported in alumina-supported 5 wt% CrO_3 catalyst calcined at 450°C the presence of mainly Cr^{6+} (580.0 eV) with a small proportion of Cr^{3+} (576.6 eV). After reduction treatment in H_2 or after carrying out the dehydrogenation of cyclohexane the same authors (34) reported an increase in the Cr^{3+} peak together with a contribution at a binding energy of 578.8 eV attributed to Cr^{5+} (33).

UV–Vis–NIR DRS characterization. Spectra of samples at increasing CrO_3 content are reported in Fig. 6. For reference, the spectra of the alumina support and of commercial α-Cr_2O_3 are given.

The sample with the lowest CrO_3 content was characterized by strong bands in the UV and Vis regions, with maxima located at about 260 and 380 nm. A shoulder at about 470 nm and a weak signal at about 715 nm were also present. In the NIR region, bands were obtained at 1390, 1893, and 2231 nm, which are attributed to the support and moisture O–H groups.

When the amount of CrO_3 was increased, the second UV peak shifted from 380 to 370 nm, and the shoulder at 470 nm became more prominent at first, so much so as to become a distinct peak, coupled with a second peak at 585 nm. An increase in the 270-nm peak followed the appearance of these bands. Finally, absorption increased in the entire NIR range, and a very broad band ranging from 800 to 2000 nm stood out in the sample with higher chromium oxide content. Such a broad band was also present in commercial samples of pure α-Cr_2O_3, as also shown in the Fig. 6. These data can be rationalized as follows:

(a) Bands at 260–270 and 380 nm are attributed to tetrahedral chromate transitions $^1T_2 \leftarrow {}^1A_1$ ($1t_1 \rightarrow 7t_2$ and $6t_2 \rightarrow 2e$) and $^1T_2 \leftarrow {}^1A_1$ ($1t_1 \rightarrow 2e$) respectively (14, 31, 36, 37).

(b) The peak at 470 nm is also assigned to a Cr^{6+} transition $^1T_1 \leftarrow {}^1A_1$ ($1t_1 \rightarrow 2e$). Since such a transition is symmetry forbidden in T_d symmetry, the intensity of this band indicates the distortion of the Cr^{6+} group from the T_d symmetry (typical of the chromate anion) caused by anchoring to the support surface, and/or the formation of a dichromate species, which has a lower symmetry than T_d

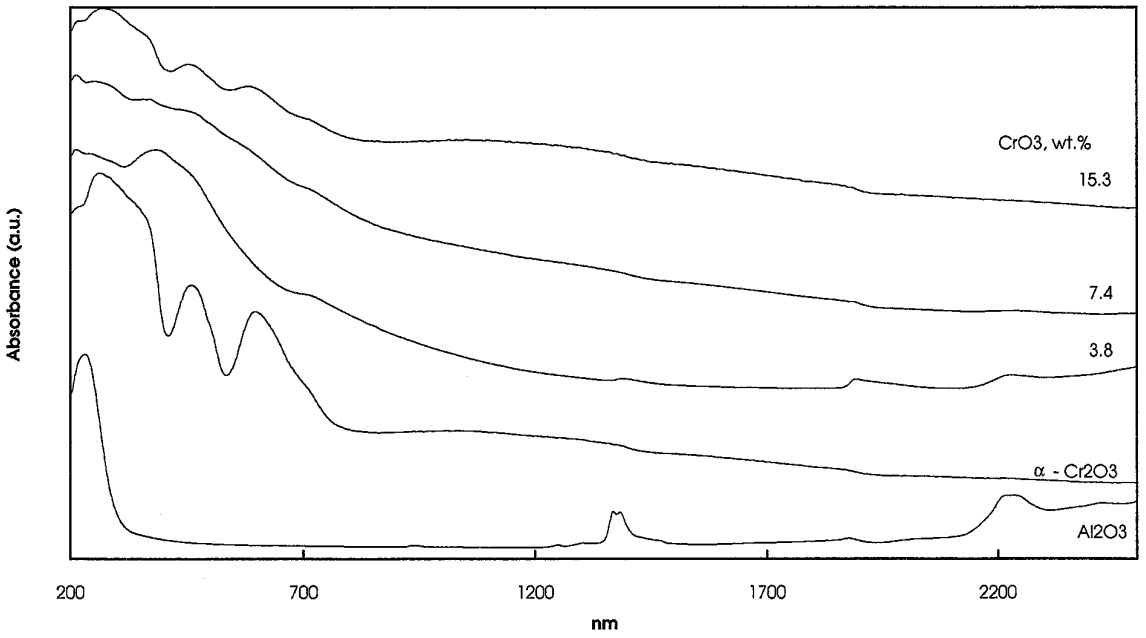

FIG. 6. UV–Vis–NIR diffuse reflectance spectra of samples at increasing CrO_3 loading and of reference compounds.

(13, 14, 38). The increase in the intensity of this peak (together with the blue-shift of the band at 380 to 370 nm) when the chromia loading was increased suggests a decrease in the symmetry of the surface chromate species. This can occur as a consequence of an increase in the extent of oligomerization, i.e., formation of dichromates (13). A different interpretation of this band has been given by other authors (14), who proposed that the state of the surface chromate species varied depending on the hydration level of the sample. In hydrated samples, CrO_4^{2-} structures were solvated by H_2O molecules, and the symmetry was almost T_d. Under dehydration, the chromate was anchored to two Al^{3+} sites, and the symmetry was lowered as demonstrated by the increase in the intensity of the forbidden transition falling at 440 nm. An increase in the latter band also occurred at increasing chromia loading, as well as a blue-shift of the two bands typical of chromates. This was explained by the authors as not due to an increase in the extent of polymerization of the chromate species, but rather to an increase in polarization (covalency) of the surface monomeric species, due to the anchoring of the less basic surface sites of alumina at high chromia loading, thus occurring as a consequence of the surface heterogeneity of alumina. In conclusion, there is not agreement on the interpretation of the band at 440–470 nm. In our case, this band was clearly observed in the 7.4 and 15.3 wt% CrO_3, samples which after calcination did not undergo any drying treatment, and therefore, according to Iannibello *et al.* (14) the band at 440 nm should be less intense than that shown in our samples. In addition, the effects observed by Iannibello *et al.* (14) were observed in samples containing much lower amounts of CrO_3 than that contained in our samples, in the range 0.5–2.3 wt% Cr, i.e., at concentrations at which alumina surface sites of different basicity can be differentiated. In our case, instead, it is likely that the amount of chromium oxide loaded is such that the observed effects can be more likely attributed to modifications in the extent of Cr^{6+} ion oligomerization.

(c) The weak band at 715 nm is of more difficult interpretation. Spin-forbidden bands of Cr^{3+} are expected in this region, since the chromate and dichromate lower energy transition is reported near 460–470 nm (14, 38). Some authors (38) have proposed that even lower energy transitions are attributable to a metal-to-ligand charge transfer transition, but this is not expected when the ligand is Al^{3+}. However, in our sample with the lowest chromium oxide content Cr^{3+} was not found by chemical analysis, and absorptions relative to octahedral Cr^{3+} are absent; indeed, the characteristic crystal field bands (32, 37) were not observed.

This band, therefore, can be assigned to a ligand field transition of chromium species having an oxidation number between (V) and (IV) (37, 39). It is known that Cr^{5+} may be present in chromium oxide lattices (40). Cr^{5+} has also been observed at a similar wavelength in silica-supported chromium oxide (41). Visible spectra of Cr^{5+} in an oleum solution (42) show a similar absorbance at 730 nm, in addition to a second peak at 550 nm. Also spectra of solid $(NH_4)_2(CrOCl_5)$ (43) show absorption peaks at 775 and 425 nm.

TABLE 3

Ligand Field Parameters of Cr^{3+} for the 15.3 wt% CrO_3 Calcined Catalyst, Undoped and Doped with Increasing Amounts of Potassium

Potassium content (wt% K_2O)	10Dq (kK[a])	B (kK[a])
0	17.2	0.45
0.21	17.0	0.47
0.42	17.1	0.46
0.84	17.1–16.9	n.o.
1.26	16.9	0.47
1.76	16.8	0.50
Reference compounds		
Cr_2O_3	16.7	0.47
Cr_2O_3 (ref. 45)	16.60–16.65	0.47–0.48
$Al_{1.99}Cr_{0.01}O_3$ (ref. 45)	18.0	0.62
$Al_{0.25}Cr_{1.75}O_3$ (ref. 45)	16.85	0.48

[a] 1 kK = 10^3 cm^{-1}.

(d) Bands in the visible (Vis) spectra at 455 and 582 nm, assigned to $^4T_{2g}$, $^4T_{1g} \leftarrow {}^4A_{2g}$ transitions, typical of Cr^{3+} in Cr_2O_3 (44), are instead observed at higher chromium oxide contents. The increase in the peak at 260 nm is due to a charge transfer band of Cr^{3+} which overlaps the Cr^{6+} signal.

Ligand field parameters of Cr^{3+} may be calculated from the two Vis bands of the sample containing 15.3 wt% CrO_3, by means of the relations (45)

$$10\mathrm{Dq} = {}^4T_{2g} \leftarrow {}^4A_{2g}$$

$$B = (\delta E/15) \times (10Dq - \delta E)/(0.8 \times 10Dq - \delta E)$$

where δE is the energy difference between the two Vis bands.

Data obtained for the sample with 15.3 wt% CrO_3 are reported in Table 3. These values are similar, but not the same as, those reported for Cr_2O_3, and differ from those of Cr^{3+} in several $Al_{2-x}Cr_xO_3$ corundum-type lattices (45); these differences allow us to exclude that the insertion of Cr^{3+} into the alumina lattice occurs to any great extent, even though the formation of small amounts of solid solution cannot be excluded. The values of the ligand field parameters would suggest that a defective Cr_2O_3 is formed.

(e) Finally, in the sample with 15.3 wt% CrO_3 a very broad band was observed in the NIR region ranging from about 800 to 1900 nm. The presence of oxidation states other than Cr^{3+} cannot be excluded (32, 37). The presence of these states together with the Cr_2O_3 may explain the difference in ligand field parameters observed (Table 3) and perhaps account for the lower degree of crystallinity, as indicated by the amount of crystalline α-Cr_2O_3 detected by X-ray diffraction, than that expected on the basis of chemical analysis.

Catalytic activity in isobutane dehydrogenation. Figure 7 reports the yield to isobutene at 470°C and at two levels of residence time, 0.3 and 1.35 s, plotted as a function of the overall CrO_3 content. Data were collected after 12 h, under conditions of stable catalytic performance. Under the conditions employed (relatively low temperature and low paraffin concentration) deactivation of the catalyst, which is known to occur quickly under industrial-like conditions, was instead negligible; this was probably due to the very low hydrocarbon partial pressure employed, as well as to the low temperature of reaction, 250°C lower than that industrially employed.

The higher residence time was long enough to reach the equilibrium conversion, while at lower residence time the equilibrium yield was not reached. The analysis of the results indicates that the activity is proportional to the CrO_3 content up to an amount of 4 wt%; in the range from 4 to 10 wt% CrO_3 the activity is again proportional to the chromia content, but with an increase in the catalytic activity trend. This increase can be detected by inspection of the data at both low and high residence time. After 10 wt% CrO_3, the activity decreases.

The yield is also given for the sample with 1.8 wt% CrO_3, after selective removal of the soluble Cr^{6+} species by the water treatment. The activity of the resulting catalyst was considerably lower than that of the untreated catalyst.

The Effect of Potassium Additions

Characterization by chemical analysis and XRD. Figure 8 reports the amounts of total Cr^{6+} and of grafted

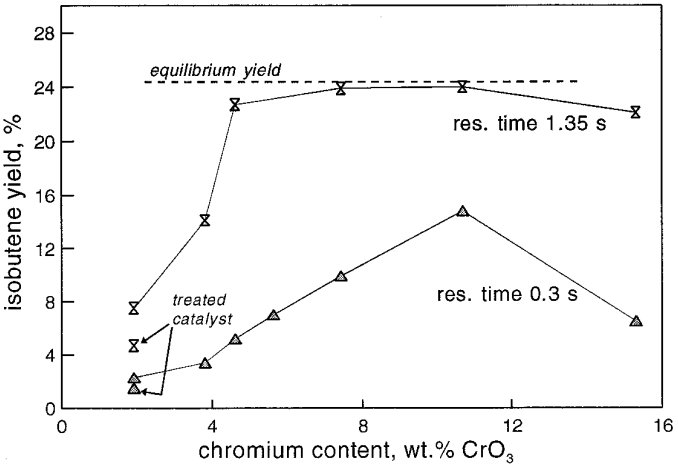

FIG. 7. Isobutene yield as a function of the chromium oxide loading in undoped catalysts, at two levels of residence time. "Treated catalyst" refers to the isobutene yield at the two levels of residence time for the catalyst treated with water.

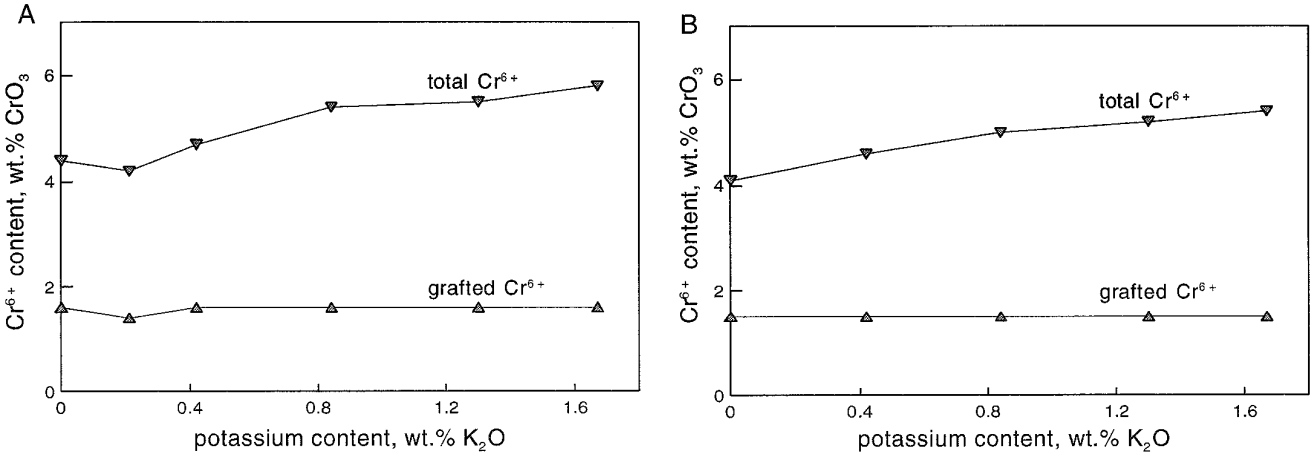

FIG. 8. Grafted and total Cr^{6+} content in the 10.6 (a) and in the 15.3 (b) wt% CrO_3 catalysts as functions of the potassium content.

Cr^{6+} determined by chemical analysis in the 10.6 (Fig. 8a) and 15.3 (Fig. 8b) wt% CrO_3-containing samples calcined at 600°C, and doped with increasing amounts of potassium (expressed as wt% K_2O). It is shown that the amount of Cr^{6+} grafted to the alumina surface is not affected by the presence of potassium. In contrast, the amount of soluble Cr^{6+} (the difference between total and grafted Cr^{6+}) increases almost linearly in the examined range of potassium concentration, while the amount of Cr^{3+} correspondingly decreases. This means that the addition of potassium leads to the formation of a Cr^{6+}-containing compound at the expense of the Cr^{3+} oxide. It is likely that the presence of potassium stabilizes the Cr^{6+} from being reduced to Cr^{3+} at the high temperature of calcination by formation of some chromate or dichromate species. Interestingly, the molar amount of Cr^{6+} that is additionally formed is approximately in a 0.4-to-1 atomic ratio with respect to the potassium, thus indicating the formation of K_2CrO_4 rather than a dichromate compound.

Also in the case of potassium-containing samples, it was not possible to titrate any amount of Cr^{6+} in catalysts after reaction.

Figure 9 shows the XRD pattern of the calcined samples containing 15.3 wt% CrO_3 and increasing amounts of K_2O. A reflection, indicated in the figure, which increased with increasing potassium content, can be assigned to a potassium chromate phase, even though a more precise attribution cannot be made, due to the impossibility to detect other reflections. The amount of crystalline α-Cr_2O_3 (4.0 $\pm$ 0.4 wt% CrO_3 at 0.21 wt% K_2O, 3.0 $\pm$ 0.3 wt% CrO_3 at 0.84 wt% K_2O, 6.8 $\pm$ 0.4 wt% CrO_3 at 1.67 wt% K_2O) initially decreases with the potassium content up to 0.84 wt% K_2O (suggesting a reaction between Cr^{6+} and potassium during the calcination treatment with formation of the potassium chromate, which prevents the formation of the α-Cr_2O_3) and then remarkably increases for the higher potassium content, indicating a possible crystallization effect of potassium on the microcrystalline or amorphous Cr^{3+} oxide to α-Cr_2O_3.

XPS characterization. Figure 10 shows the spectrum in the K 2*p* region for the 15.3 wt% CrO_3-containing catalyst doped with increasing amounts of potassium. The binding energy for the K 2*p*3/2 peak falls in the range 292.7–293.0 eV for calcined catalysts and 292.8–293.1 eV for reduced ones (Table 4). Comparable values are reported in the literature for chromate/dichromate compounds (31, 46).

The hypothesis that potassium can be involved in the formation of some chromate species seems supported by the decrease in the Cr^{3+}/Cr^{6+} intensity ratios in calcined catalysts at increasing potassium content (Table 4). The addition of potassium favors the formation of surface Cr^{6+} species at the expense of the Cr^{3+}, in agreement with the chemical analysis and XRD data. Moreover, both in the calcined and reduced catalysts a linear correlation exists

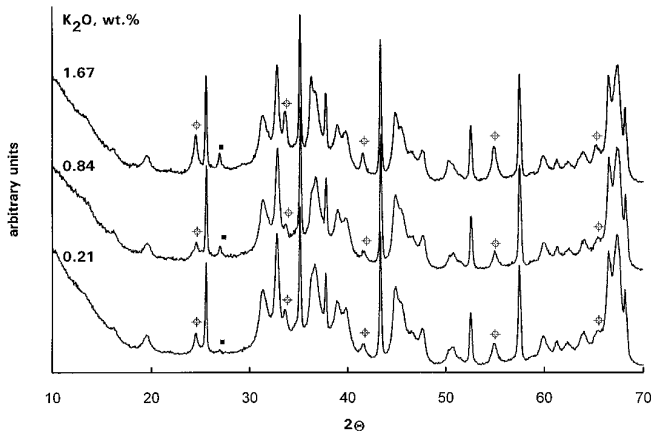

FIG. 9. X-ray diffraction patterns of calcined samples with 15.3 wt% CrO_3 and increasing potassium content ($\oplus$ α-Cr_2O_3, ■ $K_2Cr_xO_y$).

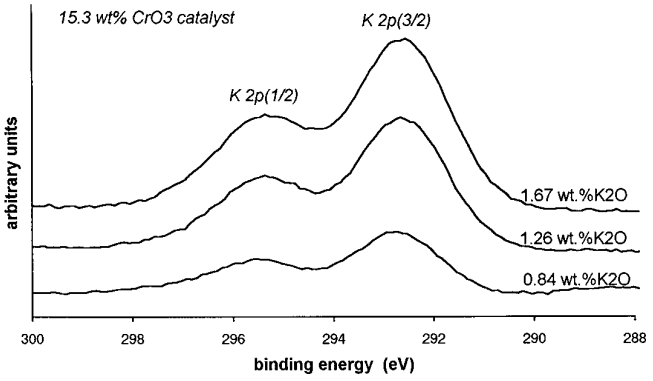

FIG. 10. XPS spectra of K 2*p* level for 15.3 wt% CrO_3 calcined catalyst at increasing K_2O loading.

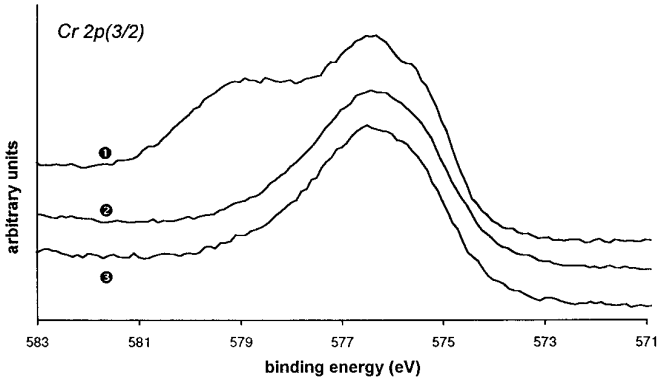

FIG. 11. Cr^{6+} signal in the Cr 2*p*3/2 spectrum for 0.84 wt% K_2O–15.3 wt% CrO_3 catalyst after calcination (1), discharged after *in situ* reduction with H_2 (2), and after reaction with 5% isobutane in He at 470°C (3).

between the intensity ratio K 2*p*/total-Cr and the bulk potassium content, as shown in Table 4. The increase in the relative intensity of potassium after reduction of Cr^{6+} can be due to a surface segregation of potassium oxide occurring by destruction of the chromate compounds.

In all potassium-containing catalysts, the Cr^{3+} state was only detected after the H_2 reduction treatment, as also found for the undoped samples discussed above. The same result was obtained for used 0.84 wt% K_2O–15.3 wt% CrO_3 catalyst discharged after reaction with 5% isobutane in He at 470°C. This is shown in Fig. 11, which compares the XPS Cr 2*p*3/2 region acquired for the calcined catalyst, before and after *in situ* H_2 treatment, and for the discharged catalyst.

Grünert *et al.* (18) found that the reduction of alumina-supported potassium-doped chromium oxide catalysts with H_2 led to an increase in the K 2*p*/Al 2*p* XPS intensity ratio and a binding energy shift (0.4 eV) for the K 2*p*3/2 toward higher values. In our case we observed the same trend, even though the shift was less pronounced. The result of Grünert *et al.* (18) was interpreted by assuming a migration of the potassium from chromate to the alumina upon reduction, in agreement also with the early results of Rozengart *et al.* (47), who described the formation of extractable potassium aluminate after reduction of oxidized Cr_2O_3/K_2O/Al_2O_3 catalyst. This also occurred with a redispersion of chromium (17, 18). In our case, due to the simultaneous increase in the K 2*p*/total-Cr XPS intensity ratio, we explain the observed behavior as a segregation of potassium oxide at the catalyst surface occurring upon reduction.

UV–Vis–NIR DRS characterization. Figure 12 shows the spectra relative to the 15.3 wt% CrO_3-containing sample doped with increasing amounts of potassium. Up to

TABLE 4

XPS Binding Energies of Undoped and Doped 15.3 wt% CrO_3 Calcined Catalysts after Different Treatments

Potassium content (wt% K_2O) and treatment	Cr^{3+} (eV[a])	Cr^{6+} (eV[a])	K 2*p*3/2 (eV)	Cr^{3+}/Cr^{6+}	K/total-Cr
0	576.7	579.3		2.7	
0, reduced at 500°C	576.4	—		—	
0.84	576.6	579.3	292.7	2.7	0.3
0.84, reduced at 500°C	576.6	—	292.8	—	0.4
0.84, after reaction at 470°C	576.7	—	292.9	—	0.3
1.26	576.8	579.4	293.0	1.9	0.5
1.26, reduced at 500°C	576.4	—	292.9	—	0.6
1.67	576.9	579.4	293.0	1.7	0.8
1.67, reduced at 500°C	576.6	—	293.1	—	0.9
		Reference compounds			
K_2CrO_4		579.1	292.1		
$K_2Cr_2O_7$		579.3	292.0		

[a] Binding energy of Cr 2*p*3/2 peak.

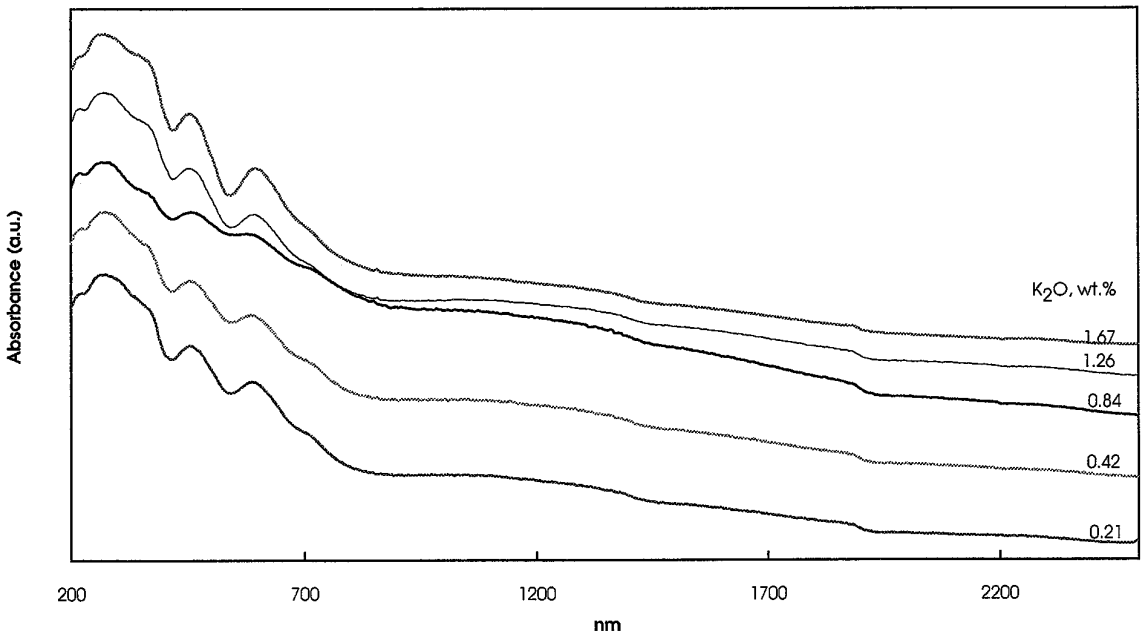

FIG. 12. UV–Vis–NIR diffuse reflectance spectra of the 15.3 wt% CrO_3 calcined catalyst containing increasing amounts of potassium.

0.84 wt% K_2O the NIR broad band became more prominent, and the Cr^{3+} ligand bands less evident. Above 0.84 wt% K_2O this trend was reversed; the NIR absorption was lowered while ligand field bands were increased. Minor changes were observed in position and intensity for the 370-nm band of Cr^{6+}. A comparison with the sample without potassium (Fig. 6) shows in the latter a less pronounced Cr^{3+} ligand field signal and a shift toward higher absolute absorption values of the broad NIR band, while maintaining its shape. Ligand field parameters obtained for Cr^{3+} (Table 3) are different from those of the undoped sample; the value of $10Dq$ becomes closer to that of crystalline α-Cr_2O_3. This agrees with the indications of the X-ray diffraction data, which evidenced an increase in the amount of crystalline α-Cr_2O_3 occurring at high potassium content. The value for the sample containing 0.84 wt% K_2O is not given because the $^4T_{2g} \leftarrow {}^4A_{2g}$ peak maximum was not well defined.

These data indicate that a double effect is induced by the addition of potassium. Up to 0.84 wt% K_2O potassium stabilizes Cr^{6+} from being reduced to Cr^{3+}, as indicated by the decrease in the intensity of the bands relative to Cr^{3+} ligand field transitions. The increase in the NIR broad band intensity can be due to an increase in the amount of mixed Cr^{3+}–Cr^{n+} $(3 < n < 6)$ valence states. Above 0.84 wt% K_2O the transformation of amorphous or microcrystalline Cr^{3+} oxide, which also contains chromium impurities at mixed valence states, to a less impure crystalline α-Cr_2O_3 leads to a decrease in the band intensity in the NIR region and to an increase in the ligand field transitions typical of Cr^{3+}, with also the ligand field parameters becoming closer to those typical of α-Cr_2O_3. Therefore, these results agree with indications obtained with the other characterization techniques.

Catalytic activity. Figure 13 shows the effect of the potassium addition on the yield to isobutene on catalysts containing 10.6 and 15.3 wt% of CrO_3. Data were collected under stationary catalytic conditions, at 470°C and 0.3 s residence time. In the former catalyst (the most active in the absence of potassium) the addition of the alkali metal leads to a continuous decrease in catalytic activity; thus, in this case chromium acts to poison activity. In the 15.3

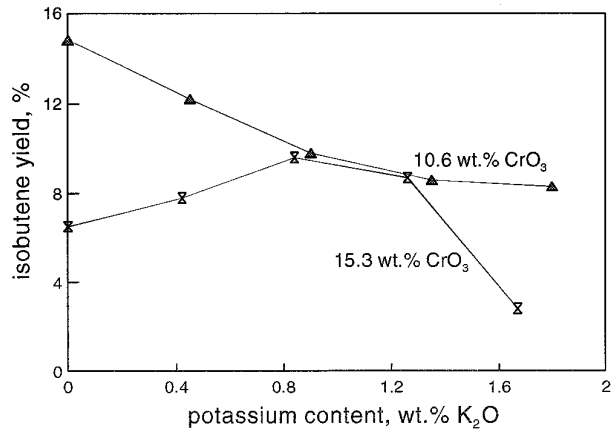

FIG. 13. Isobutene yield with 10.6 wt% CrO_3 and 15.3 wt% CrO_3 catalysts as functions of the potassium content.

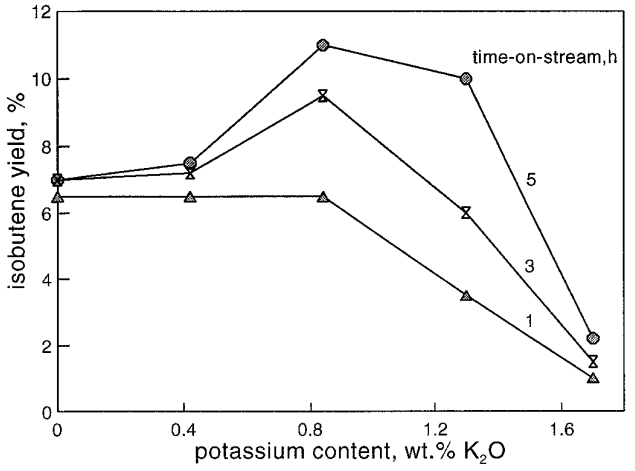

FIG. 14. Isobutene yield under nonstationary conditions after different time-on-stream values as functions of the potassium content in the 15.3 wt% CrO_3 catalyst.

wt% CrO_3 sample, instead, the activity is first increased, up to a maximum that was reached for the 0.84–1.26 wt% K_2O. Further increases in the potassium content led instead to a considerable decrease in activity.

Figure 14 plots the yield as a function of the K_2O content at different values of time-on-stream, under nonstationary conditions, for the 15.3 wt% CrO_3 catalyst. It is seen that the catalysts for which an increase in activity was finally reached exhibited an initial unstable behavior during which the yield progressively increased. This indicates that the increase in activity was due to some structural evolution which occurred during the reaction, i.e., changes occurring in the phases that are present in the potassium-doped catalysts, most likely in the potassium chromates that were formed in calcined catalysts. A hypothesis is that the destruction of the K_2CrO_4, with formation of potassium oxide or of potassium aluminate (18), accompanies the Cr^{6+} reduction, and that this phenomenon is slower than the simple Cr^{6+} reduction in undoped catalyst (in undoped catalysts initial unsteady behavior only lasts less than 1 h).

DISCUSSION

The Nature of Chromium Species in Calcined Catalysts

CrO_3 is stable at temperatures lower than 300°C; high temperatures lead to the transformation, even in air, to Cr_2O_3 (48–50). The chemistry of the supported oxide is however different from that of the bulk oxide, due to the strong interaction with the surface of the support that stabilizes different oxidation states and different coordinations of chromium. Indeed, partial reduction of Cr^{6+} also occurs when chromium oxide is supported on alumina and calcined at temperatures higher than 500°C, but the interaction between chromium and alumina stabilizes part of the chromium in the VI valence state (5, 9, 15, 47). This stabilization also occurs in the case of other supports, such as silica, zirconia and titania.

The nature of chromium species formed by deposition of chromium oxide onto a support is known to depend upon factors such as the type of support employed, the amount of deposited chromium, the degree of catalyst hydration and the temperature of calcination (6–14).

Wachs and co-workers (6–11) have made an extensive characterization of alumina-supported samples by means of laser Raman spectroscopy, a useful technique to detect the degree of condensation of chromate species. Hydrated Cr^{6+} species were found on γ-alumina, their degree of condensation being a function of the surface coverage, and more polymerized species (dichromate and trichromates) were formed with increasing chromium loading (6–10). The dehydration of surface Cr^{6+} species led to the formation of species possessing terminal Cr=O bonds (8).

Vuurman *et al.* (9) found that with a γ-alumina of 180 $m^2\ g^{-1}$ complete monolayer coverage was reached at approximately 9 wt% CrO_3, which corresponds to 0.05 wt% CrO_3 per square meter of support. Up to this amount the authors only found Cr^{6+} in catalysts calcined at 500°C, while for higher amounts crystalline Cr_2O_3 also formed.

Other authors (13, 14) instead have suggested the presence of only monomeric chromate species, on the basis of UV–Vis–NIR DRS measurements. Zaki *et al.* (13) found two types of chromate species when chromium oxide was supported on alumina, a Cr^{6+} species soluble in water and a Cr^{6+} species insoluble in water, thus anchored onto the alumina surface. The relative amounts of the former species were found to increase with overall CrO_3 content. At higher CrO_3 loadings α-Cr_2O_3 also was found.

Isolated chromate species also predominate on silica (4, 11), in a distorted tetrahedral configuration. The nature of the support, mainly its surface hydroxyl chemistry, was found to affect the nature of the degree of oligomerization of chromium species, as well as the ability to stabilize Cr^{6+} at high temperature (6).

For calcination temperatures higher than 700–800°C, or longer times at temperatures higher than 650°C, Cr^{3+} species are stabilized by forming a solid solution with alumina (9, 16).

The analyses of our samples after calcination at 600°C show the formation of different chromium species. The grafted Cr^{6+} species is the first species formed, which is anchored to the alumina surface most probably through Al–O–Cr bridges, and is probably constituted of monomeric species with T_d symmetry, according to UV–Vis–NIR DRS characterization. The maximum amount of this species is around 1.5 wt% CrO_3, and is the same for all samples examined.

The data shown in Fig. 3 indicate that an increase in the surface area leads to a proportional increase in the grafted Cr^{6+} species, thus that the fraction of covered surface is approximately constant and independent of the structural features. Some authors have proposed that the extent of surface hydroxylation may affect the nature of the chromium species that are formed (6).

The second species formed is a Cr^{6+} species that is not chemically bound to the support, but withstands the calcination treatment through an interaction with the alumina surface. This interaction is the driving force for the further spreading of the Cr^{6+} oxide (with a corresponding decrease of the Cr^{3+} oxide) onto the support once it has been selectively removed by the treatment with water and the catalyst has been newly calcined. Thus, Cr^{3+} oxide acts as a reservoir of Cr^{6+} oxide to cover the exposed surface of the alumina support. This species can be hypothesized to be constituted of polymeric groups, dispersed over the surface; its amount is around 2–2.5 wt% CrO_3.

The third species formed with increasing CrO_3 loading is Cr^{3+} oxide. Our data clearly suggest the existence of at least two different forms of Cr^{3+}. The amount of crystalline α-Cr_2O_3 determined by XRD is by far lower than the amount expected on the basis of the amount of Cr^{3+} determined by chemical analysis, suggesting the presence of Cr^{3+} oxide in an amorphous or microcrystalline phase. The latter probably also contains defects, such as chromium species in oxidation states other than III, as suggested by the DRS. This species appears only above 4 wt% CrO_3, and then increases, although not linearly, for higher CrO_3 contents.

Finally, at above approximately 7–8 wt% CrO_3, α-Cr_2O_3 also is formed. The formation of considerable amounts of Cr^{5+} in a square pyramidal configuration, together with mononuclear Cr^{6+} species, has been reported to occur in oxidized zirconia-supported chromium oxide catalysts at less than 1 wt% chromium (24). In calcined alumina-supported samples the amount of Cr^{5+} was found to be much lower (approximately 10% of the total chromium), while most chromium was present as Cr^{6+}. The formation of some amount of Cr^{5+} in calcined alumina-supported chromia catalysts has also been reported by other authors (51, 52). In our case the detection of this species by XPS is more difficult due to the relatively high amounts of chromium oxide employed and of the complexity of the signal. In any case, valence states other than Cr^{3+} and Cr^{6+} are likely present in the calcined catalysts, as suggested by the UV–Vis–NIR DRS results.

Correlation between Chromium Species and Catalytic Activity

A relationship exists between the catalytic activity and the nature of the different chromium species identified. The increase in activity observed at 4 wt% CrO_3 occurs in correspondence to the appearance in calcined catalysts of dispersed, non-XRD-detectable Cr^{3+} oxide. This suggests that this Cr^{3+} species is more active than the Cr^{3+} species that is formed in the reaction environment produced by reduction of the Cr^{6+}.

Moreover, the general increase in activity in the 0 to 10 wt% CrO_3 content range suggests that all the chromium is available for the reaction and thus accessible to the reactants. It is therefore likely that in these samples the dispersion of chromium is very high over the entire range of composition mentioned, and that therefore a sort of monolayer coverage of the alumina surface is achieved in this range. This also explains the formation of amorphous or microcrystalline Cr^{6+} and Cr^{3+} oxides, probably through an interaction with the support surface. Only when the alumina surface has been completely covered by these species do less reactive crystals of α-Cr_2O_3 build up over the spread chromium oxide, hindering access of the reactants to the underlying active coating and causing the observed decrease in activity. This confirms the general agreement that the catalytic properties of these systems are mainly related to the dispersed chromium species, rather than to the Cr^{3+} in bulk α-Cr_2O_3 (1).

In regard to the nature of the active species, in the case of propane dehydrogenation over ZrO_2-supported chromium oxide the activity per atom of chromium was found to be the same for all chromium oxide loadings (19). Analogously, in ethane dehydrogenation on chromium oxide both unsupported and supported on different oxides, Lugo and Lunsford (25) have found the same turnover frequency indicating the presence of the same type of active sites in all samples. Published data substantially suggest that whatever the initial valence state or form of aggregation of chromium, after reaching stable catalytic performance the activity is only a function of the overall chromium content.

The valence of active chromium active species, both in free Cr_2O_3 and in alumina-supported chromium oxide, has been the subject of debate for many years. According to several authors (17–19, 26, 53, 54) the active species in dehydrogenation is the Cr^{3+} ion, while for other authors either both Cr^{2+} and Cr^{3+} are active (55), or coordinatively unsaturated Cr^{2+} is active (25, 27, 28). The latter has been reported to be the active species in the case of silica-supported ethylene polymerization catalysts (2). Discrepancies in the literature can be due to differences in the physical-chemical features, but also to the fact that the reducing conditions employed can be largely different from effective reactive conditions in industrial reactors. Initial unstable catalytic behaviors are due to reaching the definite equilibrated surface composition, and the reduction of chromium may occur in periods of time which may be functions of the operating conditions. Nevertheless, there are indications in

the literature that the equilibrated operating catalyst is reduced to either Cr^{3+} or Cr^{2+} states, and that oxidized $Cr^{6+}$is no longer present.

Our data confirm the absence of oxidized chromium, and the direct relationship between dispersed chromium and activity, but further indicate that the activity of the reduced chromium species is affected by the nature of the chromium species in calcined catalysts.

Role of Alkali Metal

Figure 8 shows that for low amounts of added potassium the amount of Cr^{6+} is not modified with respect to the undoped catalyst. The first potassium added probably reacts with alumina, as also indicated by other authors (5, 18), while larger amounts may also form potassium chromates by interaction with Cr_2O_3 (16), thus explaining the increase in the soluble Cr^{6+} species observed and the corresponding decrease in the Cr^{3+} species. Characterization by spectroscopic techniques is clearly in favor of the formation of a potassium chromate phase.

Alkali metals have been indicated as promoters of activity and of selectivity for dehydrogenation reactions (5). The promotion of activity has been attributed to an increase in the number of active sites (26) and to a decrease in surface acidity. However, not all alkali metals are effective promoters, only Cs, K, and Rb. This has been attributed to a stabilization effect over the structure of alumina induced by the alkali cations that are larger in size. The increase in selectivity by destruction of the acid sites is a minor effect. Masson and Delmon (56) have reported that potassium, like rubidium and cesium, increases the intrinsic activity not directly through their basicity, but rather by increasing the number of active Cr^{3+} sites and inhibiting recrystallization of alumina to the α-phase. In the case of chromium oxide supported on ZrO_2, an inhibition effect of potassium on activity has been observed (19), but the tests were carried out only at the highest K/Cr ratios. The authors interpreted the inhibition effect of potassium as due to the fact that not only Cr^{3+} ions are the active sites, but also neighboring O^{2-} ions, which react with potassium ions. Potassium had a small beneficial effect on selectivity.

The effect of potassium reported here is rather unexpected, even though it must be said that industrial catalysts usually employ amounts of CrO_3 higher than 10 wt%, and amounts of K_2O of approximately 1 wt%, thus in the effective promoting range as shown in Fig. 13. However, the main effect of potassium is clearly to act as a poison, at least when the amount of CrO_3 is 10.6 wt%, or when the amount of K_2O is higher than 0.84 wt% for the catalyst containing 15.3 wt% CrO_3. The characterization of calcined catalysts has clearly indicated that the presence of potassium leads to the formation of a potassium chromate phase at the expense of the amorphous Cr^{3+} oxide (the prevailing Cr^{3+} species in the 10.6 wt% sample, as shown in Fig. 1), thus of the most active species. Therefore, it can be hypothesized that the Cr^{3+} species formed by destruction of the potassium chromate in the reaction environment leads to a species that is less active than the Cr^{3+} site in the dispersed Cr^{3+} oxide. In the case of the 15.6 wt% CrO_3 sample, instead, at low potassium contents the alkali metal reacts with the Cr^{6+} species thus decreasing the amount of the crystalline α-Cr_2O_3 (the intensity of the α-Cr_2O_3 reflections decreases in the XRD pattern), thus eliminating a species that is considerably less active than the amorphous Cr^{3+} oxide. Finally, at high potassium loadings, the inhibiting effect may again be due to a destruction of the most active amorphous Cr^{3+} oxide and a preferred formation of less active α-Cr_2O_3 as shown in XRD pattern in Fig. 9. Alternatively, it may be that high amounts of potassium lead to a partial coverage of the active chromium sites.

CONCLUSIONS

Model of Alumina-Supported Potassium-Doped Chromia Catalyst

On the basis of the data reported in the present work, it is possible to draw up a model for the alumina-supported potassium-doped chromium oxide catalyst after calcination. This model is illustrated in Fig. 15 for increasing amounts of CrO_3 in undoped (Fig. 15a) and doped catalysts (Fig. 15b). At low chromium oxide loading the grafted Cr^{6+} is the predominant species, which anchors to the support probably through –OH groups randomly distributed on the alumina surface. The alumina surface coverage is increased by the spreading of a Cr^{6+} oxide, which is stabilized in the higher valence state by a weak interaction with the support and is probably containing species with valence states other than VI. Further addition of chromium oxide completes the alumina coverage through the formation of microcrystalline Cr^{3+} oxide. Finally, after completion of the support coverage, α-Cr_2O_3 builds up over underlying dispersed chromium species.

The addition of potassium leads to the formation of a potassium chromate phase, with possibly some additional small amount of a potassium aluminate phase.

In the reaction environment the Cr^{6+} species is reduced to Cr^{3+}, and the potassium chromate phase is destroyed, with segregation of potassium and redispersion of the chromium. No other reduced species were detected. All the Cr^{3+} centers are active in the reaction of isobutane dehydrogenation, provided they are well dispersed on the support surface; α-Cr_2O_3 is the least active species.

The activity of the Cr^{3+} species in isobutane dehydrogenation depends on the original state of chromium in the calcined catalyst before reaction. The Cr^{3+} in dispersed Cr^{3+} oxide is the most active species, while the Cr^{3+} origi-

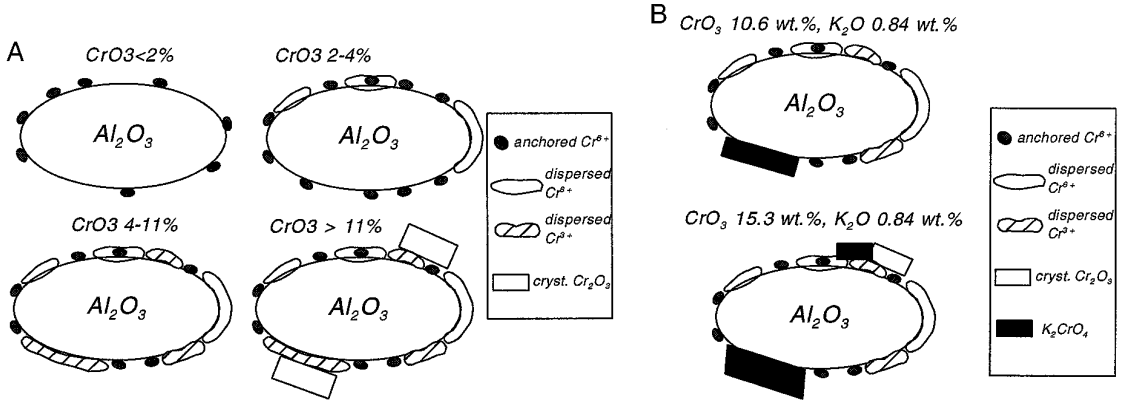

FIG. 15. Model of calcined undoped (a) and potassium-doped (b) chromium oxide-based catalysts.

nating from reduction in the reaction environment of the Cr^{6+} species is less active.

ACKNOWLEDGMENT

This work was sponsored by MURST (Ministero dell'Università e della Ricerca Scientifica).

REFERENCES

1. McDaniel, M. P., *J. Catal.* **76,** 17 and 29 (1982).
2. Merryfield, R., McDaniel, M., and Parks, G., *J. Catal.* **77,** 348 (1982).
3. Sanfilippo, D., Buonomo, F., Fusco, G., Lupieri, M., and Miracca, I., *Chem. Eng. Sci.* **47,** 2313 (1992).
4. Kim, D. S., and Wachs, I. E., *J. Catal.* **142,** 166 (1993).
5. Carrà, S., and Forni, L., *Catal. Rev. Sci. Eng.* **5,** 159 (1971).
6. Hardcastle, F. D., and Wachs, I. E., *J. Mol. Catal.* **46,** 173 (1988).
7. Vuurman, M. A., Stufkens, D. J., Oskam, A., Moulijn, J. A., and Kapteijn, F., *J. Mol. Catal.* **60,** 83 (1990).
8. Vuurman, M. A., Wachs, I. E., Stufkens D. J., and Oskam, A., *J. Mol. Catal.* **80,** 209 (1993).
9. Vuurman, M. A., Hardcastle, F. D., and Wachs, I. E., *J. Mol. Catal.* **84,** 193 (1993).
10. Vuurman, M. A., and Wachs, I. E., *J. Phys. Chem.* **96,** 5008 (1992).
11. Kim, D. S., Tatibouet, J. M., and Wachs, I. E., *J. Catal.* **136,** 209 (1992).
12. Richter, M., Reich, P., and Öhlmann, G., *J. Mol. Catal.* **46,** 79 (1988).
13. Zaki, M. I., Fouad, N. E., Leyrer, J., and Knözinger, H., *Appl. Catal.* **21,** 359 (1986).
14. Iannibello, A., Marengo, S., Tittarelli, P., Morelli, G., and Zecchina, A., *J. Chem. Soc., Faraday Trans. 1* **80,** 2209 (1984).
15. Poole, C. P., and Mac Iver, D. S., *Adv. Catal.* **17,** 223 (1967).
16. Bremer, H., Muche, J., and Wilde, M., *Z. Anorg. Allg. Chem.* **497,** 40 (1974).
17. Grünert, W., Saffert, W., Feldhaus, R., and Anders, K., *J. Catal.* **99,** 149 (1986).
18. Grünert, W., Shpiro, E. S., Feldhaus, R., Anders, K., Antoshin, G. V., and Minachev, Kh. M., *J. Catal.* **100,** 138 (1986).
19. De Rossi, S., Ferraris, G., Fremiotti, S., Cimino, A., and Indovina, V., *Appl. Catal. A. General* **81,** 113 (1992).
20. Cordischi, D., Indovina, V., and Occhiuzzi, M., *Appl. Surf. Sci.* **55,** 233 (1992).
21. De Rossi, S., Ferraris, G., Fremiotti, S., Indovina, V., and Cimino, A., *Appl. Catal. A: General* **106,** 125 (1993).
22. Gazzoli, D., Occhiuzii, M., Cimino, A., Minelli, G., and Valigi, M., *Surf. Interface Anal.* **18,** 315 (1992).
23. Cordischi, D., Campa, M. C., Indovina, V., and Occhiuzzi, M., *J. Chem. Soc. Faraday Trans. 1* **90,** 207 (1994).
24. Cimino, A., Cordischi, D., De Rossi, S., Ferraris, G., Gazzoli, D., Indovina, V., Minelli, G., Occhiuzzi, M., and Valigi, M., *J. Catal.* **127,** 744 (1991).
25. Lugo, H. J., and Lunsford, J. H., *J. Catal.* **91,** 155 (1985).
26. Marcilly, Ch., and Delmon B., *J. Catal.* **24,** 336 (1972).
27. Slovetskaya, K. I., and Rubinstein, A. H., *Kinet. Katal.* **9,** 1115 (1968).
28. van Reijen, L. L., Sachtler, W. M. H., Cossee, P., and Brouwer, D. M., *in* "Proceedings, 3rd International Congress on Catalysis, Amsterdam, 1964" (W. M. H. Sachtler, G. C. A. Schuit and P. Zwietering, Eds.), p. 829. North Holland, Amsterdam, 1965.
29. Chung, F. H., *J. Appl. Crystallogr.* **7,** 519 (1974).
30. Allen, G. C., and Tucker P. M., *Inorg. Chim. Acta* **16,** 41 (1976).
31. Allen, G. C., Curtis, M. T., Hooper, A. J., and Tucker, P. H., *J. Chem. Soc. Dalton Trans.* 1675 (1973).
32. Cimino, A., De Angelis, B. A., Lucchetti, A., and Minelli, G., *J. Catal.* **45,** 316 (1976).
33. Okamoto, Y., Fuiji, M., Imanaka, T., and Teranishi, S., *Bull. Chem. Soc. Jpn.* **49,** 859 (1976).
34. Jagannathan K., Srinivasan, A., and Rao, C. N. R., *J. Catal.* **69,** 418 (1981).
35. Best, S. A., Squires, R. G., and Walton, R. A., *J. Catal.* **47,** 292 (1977).
36. Scofield, J. H., *J. Electron Spectrosc.* **8,** 129 (1976).
37. Schoonheydt, R. A., *in* "Characterization of Heterogeneous Catalysts" (F. Delannay, Ed.), p. 125. Dekker, New York, 1984.
38. Szabo, Z. G., Kamaras, K., Szebeni, Sz., and Ruff, I., *Spectrochim. Acta* **34A,** 607 (1978).
39. Ellison, A., Oubridge, J. O. V., and Sing, K. S. W., *J. Chem. Soc., Faraday Trans. 1* **66,** 1004 (1970).
40. Cotton, F. A., and Wilkinson, G., "Advanced Inorganic Chemistry, 4th Ed." p. 732. Wiley, New York, 1980.
41. Zecchina, A., Garrone, E., Chiotti, G., Morterra C., and Borello, E., *J. Phys. Chem.* **79,** 966 (1975).
42. Mishra, H. C., and Symons, M. C. R., *J. Chem. Soc.* 4490 (1963).
43. Gray, H. B., and Hare, C. R., *Inorg. Chem.* **1,** 363 (1962).
44. Poole, C. P., and Itzel, J. F., *J. Chem. Phys.* **39,** 3445 (1963).
45. Reinen, D., *in* "Structure and Bonding" Vol. 6, p. 31. Springer-Verlag, Berlin, 1969.
46. Nefedov, V. I., Salyn, Y. V., Solozhenkin, P. M., and Pulatov, G. Y., *Surf. Interface Anal.* **2,** 171 (1980).
47. Rozengart M. I., Kuznetsova, Z. F., and Gitis, K. M., *Neftekhimiya* **5,** 17 (1965).

48. Bencovski, A., Caraman, A., Fatu, D., Pop, E., Segal, E., and Serban, Gh., *J. Therm. Anal.* **5,** 427 (1973).
49. Kubota, B., *J. Am. Ceram. Soc.* **44,** 239 (1961).
50. Glemser, O., Hauschild, U., and Trupel, F., *Z. Anorg. Allg. Chem.* **277,** 113 (1954).
51. van Reijen, L. L., Cossee, P., and van Haren, H. J., *J. Chem. Phys.* **38,** 572 (1963).
52. van Reijen, L. L., and Cossee, P., *Disc. Faraday Soc.* **41,** 277 (1966).
53. König, P., and Tétényi, P., *Acta Chim. Acad. Sci. Hung.* **89,** 123 and 137 (1976).
54. Shvets, V. A., and Kazanskii, V. B., *Kinet. Katal.* **7,** 712 (1966).
55. Ashmawy, F. M., *J. Chem. Soc., Faraday Trans. 1* **76,** 2096 (1980).
56. Masson, J., and Delmon, B., ''Proceedings, 5th Internation Congress on Catalysis, Palm Beach, 1972'' (J. W. Hightower, Ed.). **2,** 183. North Holland, Amsterdam, 1973.